Proceedings of the 7th International Young Geotechnical Engineers Conference – Scott (Ed.)

Triaxial tests on carbonated cement samples with bacterial nanocellulose in the context of carbon capture and storage

Essais triaxiaux sur des échantillons de ciment carbonaté avec de la nanocellulose bactérienne dans le contexte du captage et du stockage du carbone

Juan Cruz Barría, Sandra Orlandi, Ricardo Guerreiro & Diego Manzanal
Laboratorio de Investigación de Suelos, Hormigones y Asfaltos, Universidad Nacional de la Patagonia San Juan Bosco, Argentina, juan-cruz.barria@enpc.fr

Siavash Ghabezloo & Jean-Michel Pereira
Navier, École des Ponts, Univ. Gustave Eiffel, CNRS, France

Diego Manzanal
E.T.S.I. de Caminos, Canales y Puertos, Universidad Politécnica de Madrid, Spain.

ABSTRACT: The carbon capture and storage (CCS) technology covers various processes to mitigate the emission of carbon dioxide (CO_2) into the atmosphere. Geological reservoirs are suitable for storage. The system consists of a steel pipe aligned with the well and a cement ring section, which protects the steel pipe from corrosion and provides well integrity. Once the gas is injected, the well is sealed to prevent the passage of CO_2 to other formations or to the surface. In the long term, cement begins to carbonate, modifying its mechanical properties. The cement will be then subjected to supercritical carbonation due to the high pressure and temperature conditions of the reservoir. The effect of carbonation on modified cement with bacterial nanocellulose was studied in the laboratory at high pressure and temperature. Furthermore, isotropic triaxial tests were carried out to determine their elastic properties. Additionally, a chemo-hydro-mechanical model was used to implement the development of damage through the sample. Experimental results show that the sample reduces its mechanical properties, and the damage model shows the reduction of the elastic modulus of the sample.

RÉSUMÉ : La technologie du captage et du stockage du carbone (CSC) couvre une série de procédés visant à atténuer les émissions de dioxyde de carbone (CO_2) dans l'atmosphère. Les réservoirs géologiques se prêtent au stockage. Le système se compose d'un tuyau en acier aligné sur le puits et d'une section annulaire en ciment, qui protège le tuyau en acier de la corrosion et assure l'intégrité du puits. Une fois le gaz injecté, le puits est scellé pour empêcher le passage du CO_2 vers d'autres formations ou vers la surface. À long terme, le ciment commence à se carbonater, ce qui modifie ses propriétés mécaniques. Le ciment sera alors soumis à une carbonatation supercritique en raison des conditions de pression et de température élevées du réservoir. L'effet de la carbonatation sur le ciment modifié avec de la nanocellulose bactérienne a été étudié en laboratoire à haute pression et température. Des tests triaxiaux isotropes ont été réalisés pour déterminer leurs propriétés élastiques. De plus, un modèle chimio-hydro-mécanique a été utilisé pour mettre en œuvre le développement des dommages à travers l'échantillon. Les résultats expérimentaux montrent que l'échantillon réduit ses propriétés mécaniques et le modèle d'endommagement montre la réduction du module élastique de l'échantillon.

KEYWORDS: CO_2 geological storage, cement paste, bacterial nanocellulose, triaxial tests, damage

1 INTRODUCTION

New technologies are allowing the reduction of CO_2 concentration in the atmosphere. One of these technologies is carbon capture and storage (CCS) technology (Ringrose, 2020). The gas emitted by the companies can be redirected and injected underground in geological reservoirs. These reservoirs have a large volume suitable for storing these gases. Nevertheless, this implies that the gases stored do not leak out from this reservoir.

The first part studies the behavior of the formation under CO_2 injection and the second part studies the long-term behavior. Long term behavior is essential for the proper functioning of the system. The drilled wellbore is filled with a concentric steel casing and cement between the casing and formation. Cement provides isolation of the casing from harmful fluids in the formation and maintains the structural integrity of the wellbore.

The CO_2 injected into the reservoir begins to carbonate the cement, modifying its chemical structure andits mechanical behavior. The components affected are calcium hydroxide (CH) (Eq. 1) and hydrated calcium silicate (C-S-H) (Eq. 2). This reaction causes calcium carbonates (CC) to precipitate and form amorphous silica (AmSi) in the cement (Fernández et al., 2004).

$$\mathrm{CH} + \mathrm{CO_2} \rightarrow \mathrm{CC} + \mathrm{H_2O} \quad (1)$$

$$\mathrm{C-S-H} + 1.7\ \mathrm{CO_2} \rightarrow 1.7\ \mathrm{CC} + \mathrm{AmSi} \quad (2)$$

In addition, the pressure and temperature in the reservoir cause the CO_2 to be in a supercritical state. This improves cement carbonation since the CO_2 concentration in the fluid is higher, and its viscosity is similar to gas.

The discontinuities produced and the changes in the chemical components of the cement can compromise the integrity of the well.

Nowadays, different types of cement are being tested to improve its performance against carbonation. Previous works have shown that bacterial nanocellulose can be a feasible alternative in this case (Gómez Hoyos et al., 2013; Mejdoub et al., 2017). In addition, these fibers retain water allowing further hydration compared with non-modified cement (Hisseine et al., 2018).

This work aims to study the variation of the compressibility modulus of cement in drained and undrained conditions once it is subjected to carbonation at a pressure of 20 MPa and at a

temperature of 90°C. This is carried out through isotropic tests in a high-pressure triaxial cellule.

A numerical simulation of carbonation is also presented using the finite element method with a chemo-hydro-mechanical coupling. The isotropic damage calculation is implemented to obtain the elastic modulus. A deviatoric case is simulated to show the elastic modulus variation after a mechanical loading and carbonation.

2 MATERIALS AND METHODS

Cement samples were prepared according to the American Petroleum Institute standard 10A (API Specification 10A, 2019). Two different mixtures were used. One was Portland cement with no additives (PC), and the other contained 0.05% of bacterial nanocellulose (BNC05). The BNC membranes were wet-grinded and mixed with distilled water in order to obtain a suitable additive. This additive was then conditioned in an ultrasound bath for 30 min at 40.000 Hz to obtain a better dispersion of the BNC fibers (Barría et al., 2021). The necessary water for mixing was then calculated to obtain a water to cement ratio of 0.44.

The slurry was poured into cylindrical molds for 24 h and then removed from the mold. Later, they were cured for 28 days in water at 20°C (Barría et al., 2020a). Once removed from the batch, they were cut with a diamond saw to obtain cylindrical samples of 38x76 mm.

2.1 *Carbonation*

Carbonation was performed in a titanium cell at 20 MPa and 90°C in static conditions. Water was poured into the bottom of the cellule to maintain a wet atmosphere. The fluid in contact with the samples was wet-supercritical CO_2. As presented in previous works, the samples were allowed to carbonate for 30 days (Barría et al., 2020a). Figure 1 shows the carbonation system.

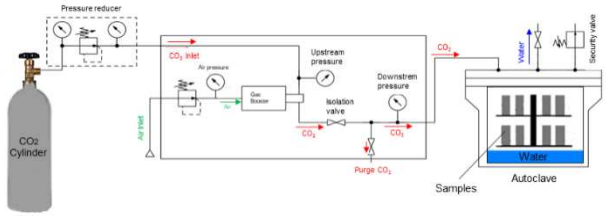

Figure 1. Carbonation system

2.2 *Triaxial tests*

Triaxial tests were performed in cement samples to determine the compressibility modulus at different confinement conditions, simulating underground conditions.

Cylindrical cement samples of 38 mm in diameter and 78 mm long were placed inside a neoprene membrane. Two linear variable differential transformers (LVDT) were positioned in the axial direction and four in the radial direction touching a thin aluminum sheet glued to the four radial pierced holes in the membrane.

At the top and bottom of the sample, porous stones were placed to allow a homogeneous pore pressure distribution. Pore pressure and confinement pressure were measured by electronic transducers and controlled by software linked to hydraulic pumps.

The tests performed were:

- Undrained isotropic tests
- Drained isotropic tests

The isotropic tests were performed with initial confinement values ranging from 5 to 30 MPa. The isotropic load increases to a certain value and then unloads to the initial value. The compressibility modulus of the sample is measured from the load curve.

In the undrained isotropic test, the pore pressure exit valve is closed, not allowing mass exchange. In this case, the increase in pore pressure within the sample is measured through pressure sensors. While for the drained isotropic test, the exit valve is open to let the water evacuate from the sample.

The parameters obtained during triaxial tests were the undrained bulk modulus (Ku) and drained bulk modulus (Kd)

3 RESULTS

Figure 2 shows the samples affected after 30 days of carbonation. Some of the samples were damaged and broken during the tests, probably due to depressurization.

Density increases from 1.99 to 2.07 g/cm^3 with a mass uptake average of 2.7 g per sample. For BNC05, the initial density was 1.93 g/cm^3, and the density of the carbonated samples was 2.02 g/cm^3. This is a result of the higher density of carbonates compared to CH, and due to the higher amount of CC produced in the reaction of Eq. 1 with a CC/C-S-H ratio of 1.7. Even though the density of BNC05 is lower than PC samples, previous works have demonstrated that the uniaxial compression strength was higher for BNC05 samples (Barría et al., 2020a).

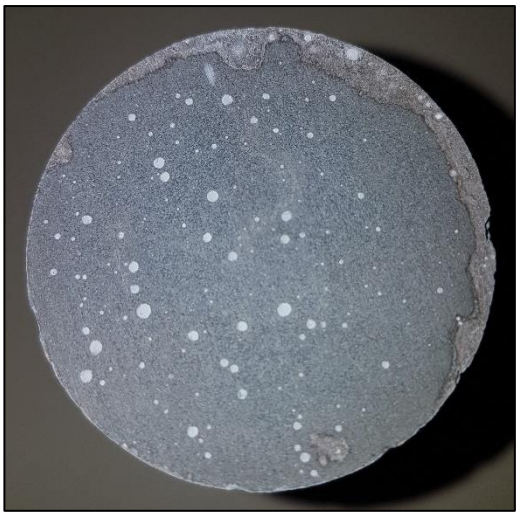

Figure 2. BNC05 sample after 30 days of supercritical carbonation at 20MPa and 90°C. The white points are capillary pores.

The isotropic tests of non-carbonated samples are shown in Figure 3. The x-axis indicates the initial confinement pressure at the time of the tests, andthe y-axis indicates the drained or undrained value of the compressibility modulus for that initial confinement.

The undrained slopes are steeper than the drained slopes, and the values of drained and undrained compressibility modulus are similar to previous values obtained in the literature (Ghabezloo et al., 2008; Samudio, 2018).

The increment in the bulk modulus when the initial confinement pressure is higher indicates that the elastic properties are dependent on the initial stress state of the sample. Indeed, in a poroelastic material, the pore structure varies depending on the stress state. Thus, if the confinement increases, the pore structure is reduced, and there is more solid material per unit of volume available to resist the new stress state.

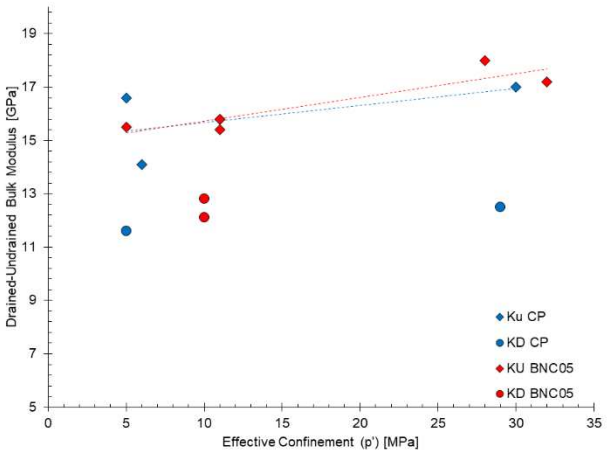

Figure 3. Bulk modulus of drained (Kd) and undrained (Ku) tests on non-carbonated (NC) samples. Results are shown according to the initial confinement pressure of each test.

Samples with BNC present a slight increment compared to those with no BNC content. The undrained modulus increases from 15.30 for PC to 16.30 for BNC05. The Skempton coefficient was 0.33. An increase of 0.50 GPa is observed in the drained modulus for samples with the addition of BNC. The increase of this value is related to the effect of bacterial nanocellulose that allows higher cement hydration. The bacterial nanocellulose fibers have high tensile strength, which may reduce the cracks caused by cement shrinkage (Gatenholm and Klemm, 2010).

Figure 4 shows the bulk modulus of the carbonated samples.

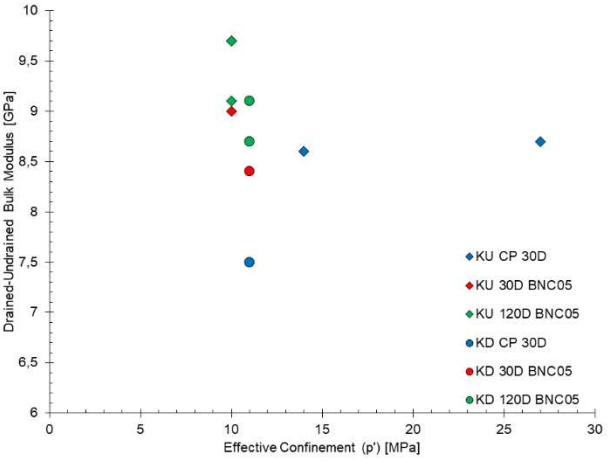

Figure 4. Bulk modulus of drained (Kd) and undrained (Ku) tests on carbonated (C) samples. Results are shown according to the initial confinement pressure of each test.

The outer rim of the carbonation samples is affected and presents different discontinuities, which could allow higher deformations when an isotropic loading is applied.

Carbonation generates different fronts: leaching, precipitation, and re-dissolution) (Kutchko et al., 2008). These discontinuities in cement reduced the mechanical properties of cement (Xu et al., 2019)

Additionally, the exterior front of re-dissolution is characterized by its large porosity due to calcite leaching. This layer behaves in a more compressible way than the others. When the external confinement is varied, a more significant volumetric variation of the sample is observed, decreasing the bulk modulus.

The average values obtained from all the isotropic tests are shown below. Table 1 shows the bulk modulus of PC samples, while Table 2 shows the bulk modulus of BNC05 samples. Carbonation reduces drained and undrained bulk moduli by up to 40% for both mixtures.

Table 1. Average bulk modulus values of PC obtained from isotropic tests at different confinement pressures

Measured parameter	*Non-carbonated*	*Carbonated*
Ku [GPa]	15.30	8.60
Kd [GPa]	12.00	7.50

Table 2. Average bulk modulus values of BNC05 obtained from isotropic tests at different confinement pressures

Measured parameter	*Non-carbonated*	*Carbonated*
Ku [GPa]	16.30	9.40
Kd [GPa]	12.50	8.70

4 NUMERICAL ANALYSIS

4.1 *Fundamentals*

The experimental tests are simulated with a chemo-hydro-mechanical coupled model (Vallin et al., 2013) implemented in a finite element code called BIL 2.3.0 (Dangla and Bonnard, 2017).

The carbonation advance in 1D or 2D materials can be represented. The model contains the balance equations of equilibrium of the continuum mechanics based on mass conservation, momentum, and energy (Vallin, 2014).

For the model, cement is considered a porous multiphase material composed of a solid matrix and water-saturated pores. The skeleton is composed of different materials, such as calcium hydroxide (CH), calcium silicate hydrate (C-S-H), aluminates, and calcite (CC).

CO_2 is considered dissolved in the aqueous solution. The chemical reactions start when the CO_2 concentration reaches a specific value. The chemical reactions are assumed to be instantaneous (Vallin et al., 2013).

The CH is the first cement hydrated to react with CO_2 and precipitates CC. Once the pH level of the solution drops below 9, the carbonation will start to consume the C-S-H, also precipitating CC and amorphous silica (Morandeau et al., 2014).

The model considers an elastic isotropic porous material of an infinitesimal representative volume element. The poroelastic balance in isothermal conditions are the following (Eq. 3, 4, 5, 6):

$$\boldsymbol{\sigma} - \boldsymbol{\sigma_0} = \left(\mathrm{K} - \frac{2}{3}\mathrm{G}\right)(\varepsilon - \varepsilon_0)\mathbf{1} + 2\mathrm{G}(\boldsymbol{\varepsilon} - \boldsymbol{\varepsilon_0}) - \sum_{\mathrm{k=F,C}} \mathrm{b_k}(\mathrm{p_k} - \mathrm{p_{k,0}})\mathbf{1} \quad (3)$$

$$\varphi_J - \varphi_{J,0} = b_J(\varepsilon - \varepsilon_0) + \sum_{k=F,C} \frac{p_k - p_{k,0}}{N_{JK}}; J = F, C \quad (4)$$

Where:

$\boldsymbol{\sigma}$: Stress tensor

$\boldsymbol{\varepsilon}$: Infinitesimal strain tensor

ε: Volumetric strain. ($\mathrm{tr}(\boldsymbol{\varepsilon})$)

K, G = Bulk and shear modulus in drained conditions

φ_J: Porous volume deformation occupied by the phase J

b_J: Generalized Biot coefficient

N_{JK}: Generalized poroelastic coupling moduli (Coussy, 2010).

The mass conservation is applied to the fluid and to the molar amount of CO_2

$$\left(\frac{\rho_f \phi_f}{K_f} + \frac{\rho_f}{N_{FF}}\right)\frac{\partial p_f}{\partial t} + \rho_f b\ div\ \left(\frac{\partial \boldsymbol{u}}{\partial t}\right) + \rho_f \sum_{R_i} Y_{Ri} \frac{\partial \xi_{Ri}}{\partial t} -$$

$$div\left(\rho_f \frac{\kappa}{\eta} grad\ \rho_f\right) = 0 \quad (5)$$

$$\frac{\partial(\phi_f\, c_{CO_2})}{\partial t} + \sum_{R_i} a_{Ri} \frac{\partial \xi_{Ri}}{\partial t} - div\left(d_{eff}\, \boldsymbol{grad}\, c_{CO_2} +\right.$$

$$\left. c_{CO_2} \frac{\kappa}{\eta} \boldsymbol{grad}\, \rho_f\right) = 0 \quad (6)$$

Where:

ρ_f is the density of the fluid.

ϕ_f is the fluid porosity.

K_f is the bulk modulus of the fluid.

p_f is the fluid pressure.

a_{Ri} is the stoichiometric coefficient of the reaction Ri

c_{CO_2} is the CO_2 concentration in fluid.

η is the dynamic viscosity of the fluid phase.

Y_{Ri} is a variable that depends on the molar volumes of reactive species

$\boldsymbol{u}$ is the skeleton displacement vector.

ξ_{Ri} is the reaction advance depending on κ and d_{eff}, which are the permeability and diffusion coefficients.

Diffusion and permeability transport phenomena control the carbonation advance (Ghabezloo et al., 2009; Mainguy, 1999).

4.2 *Homogenization of the poroelastic parameters*

The model performs a homogenization of the medium to determine the bulk properties of the specimen, including the fluid. The poroelastic parameters can then be simplified following the relations (Eq. 7, 8, 9, 10) (Ulm et al., 2004):

$$K_d^{hom} = \sum_r f_r k_r A_r^v \quad (7)$$

$$G_d^{hom} = \sum_r f_r g_r A_r^d \quad (8)$$

$$b^{hom} = 1 - \sum_r f_r A_r^v \quad (9)$$

$$\frac{1}{N^{hom}} = \sum_r f_r \frac{1 - A_r^v}{k_r} \quad (10)$$

Where K_d^{hom} is the drained bulk modulus, G_d^{hom} is the drained shear modulus, b^{hom} is Biot's parameter, N^{hom} is the Biot skeleton modulus, f_r is the volumetric proportion of the phase r, k_r and g_r are the elastic parameters of the solids r and A_r^v and A_r^d are the volumetric and deviatoric strain localization coefficients. A homogenization formulation was implemented for this case, adding the BNC characteristics (Barría et al., 2019, 2018).

As carbonation advances, homogenization allows us to know the poroelastic parameters of the cement paste in each step of time.

4.3 *Isotropic damage*

From a microscopic point of view, the damage corresponds to the creation of microcracks. In the theory of damage, effective stress, now called damaged stress, is based on a decrease of the effective area due to the appearance of micro-cavities (Kachanov, 1971). Considering damage as isotropic, a simplification for calculating the damaged stress can be made (Eq. 11):

$$\tilde{\boldsymbol{\sigma}} = \frac{\boldsymbol{\sigma}'}{1-d} \quad (11)$$

When d = 0, there is no damage. When damage is between 0 and 1, the material is in a damaged state. If d = 1, the material is broken.

The interior of the yield surface ($f_d < 0$) corresponds to the effective stress space for which no damage occurs, and the exterior ($f_d > 0$) the space for which the effective stress state cannot be reached. Thus, as long as the stress state remains within the damaged surface, the damage will not evolve. Similarly, if the stress state reaches the loading surface, but the material point understudy is subjected to unloading, there will be no evolution of the damage. On the other hand, if the stress state is on the yield surface and the loading increases, the damage will increase.

The model adopts a Drücker-Prager criterion (Eq. 12), suitable for the behavior of high confinement geomaterials (Vallin, 2014). The criterion takes the following form:

$$f_d = q + ff\sigma_m - cc \quad (12)$$

Where ff and cc are parameters depending on the friction angle of the material and its cohesion, while q and σ_m are the deviatoric stress and effective mean stress.

4.4 *Damage evolution*

The mean and deviatoric stresses are evaluated from the imposed deformation and the homogenized modulus (Eq. 13 and Eq. 14):

$$\sigma_m = \sigma_{m0} + K_d^{hom} \Delta\varepsilon_v \quad (13)$$

$$q = q_0 + G_d^{hom} \Delta\varepsilon_s \quad (14)$$

With $\varepsilon_v = Tr(\boldsymbol{\varepsilon})$ and $\varepsilon_s = \sqrt{\frac{2}{3} J_{2\varepsilon}}$. $\Delta\varepsilon_v$ and $\Delta\varepsilon_s$ are the increments of the volumetric and deviatoric strains.

Once the stress state reaches the Drücker-Prager criterion and f_d is greater than zero, the damage is calculated in function of an increment of deviatoric and volumetric deformations (Eq. 15):

$$d_{n+1} = 1 - \frac{cc - q - ff\sigma_m}{3G_c^{hom}\Delta\varepsilon_s + ff K_c^{hom} \Delta\varepsilon_v} \quad (15)$$

Where K_c^{hom} and G_c^{hom} are the compressibility and shear modulus of the homogenized medium right before reaching the criterion. And the new damaged stress state will be (Eq. 16):

$$\boldsymbol{\sigma'} = \boldsymbol{\sigma_0} + (1 - d_{n+1})\left(2G_c^{hom}(\boldsymbol{\varepsilon} - \boldsymbol{\varepsilon_0}) + \left(K_c^{hom} - \frac{2}{3} G_c^{hom}\right)(tr(\varepsilon) - tr(\varepsilon_0))\mathbf{1}\right) \quad (16)$$

Finally, in a simplified way, the mechanical modulus is affected as Eq. 17 describes:

$$K = (1 - d) K_d^{hom} \quad (17)$$

4.5 *Chosen geometry and boundary conditions*

The geometry chosen is one-quarter of the testing cement samples. This geometry will be tested at a confinement of 20 MPa and a temperature of 90°C. As the code is not thermally coupled, the fluid and gas conditions are set at a temperature of 90°C. First, initial damage is applied to the sample by a deviatoric loading, then it is carbonated with a molarity of 1.5, and finally, it is tested until failure with a deviatoric loading. This loading and carbonation path is adopted to show the effect of damage and carbonation separately.

A 2D rectangular shape model was used to simulate the carbonation advance in these samples. The rectangular shape consisted of one-quarter of a sample (19 mm-radius by 38 mm-height) using a mesh of 22x11 elements (Figure 5). The bottom horizontal contour has restricted movements in the X direction,

while the left vertical contour has restricted movements in the Y direction. The top and right-hand contours are subjected to the carbonation of the cell and with liquid pressure as a boundary condition.

The boundary conditions adopted are based on the carbonation technique, and the triaxial test carried out in the laboratory:

- Triaxial test: Isotropic confinement at 20 MPa and a pore pressure of 5 MPa
- Initial damage by deviatoric loading-unloading
- 30 days of carbonation at 20 MPa and 90°C
- Deviatoric test until failure.

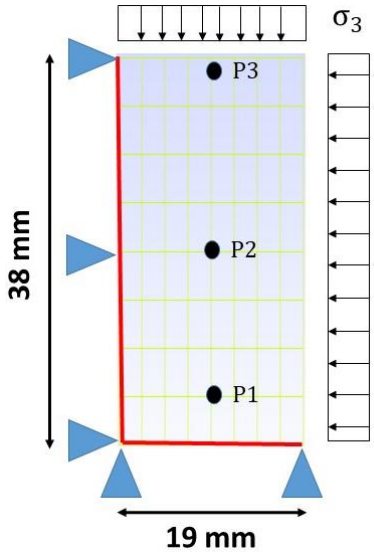

Figure 5. Geometry considered for the model

The results of the mechanical tests presented were placed as inputs in the model, such as bulk modulus and Skempton coefficient. The maximum strength and initial porosity were taken from previous work (Barría et al., 2019, 2018).

Figure 6 shows the carbonation advance of point P3. Initially, all the calcium hydroxide is depleted, and the C-S-H carbonation starts. As the carbonation continues, the C-S-H is also depleted, and only calcium carbonates are the only minerals remaining.

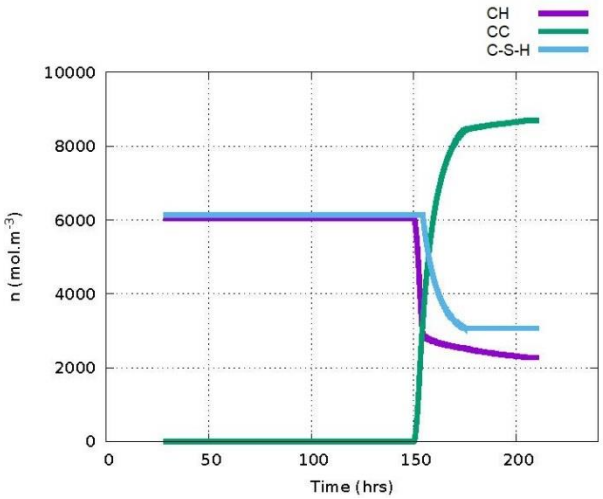

Figure 6. Geometry considered for the model

This allows the carbonation of P3 and the variation of its bulk modulus over time as Figure 7 shows. First, an increase in the K_d^{hom} is observed due to pore compressibility, and later it drops due to the damage caused by the mechanical loading. Once the carbonation begins, the bulk modulus suffers a slight increase while the CH is being carbonated, but it begins to decrease when the C-S-H is leached. Finally, the new mechanical loading increases it slightly before failure.

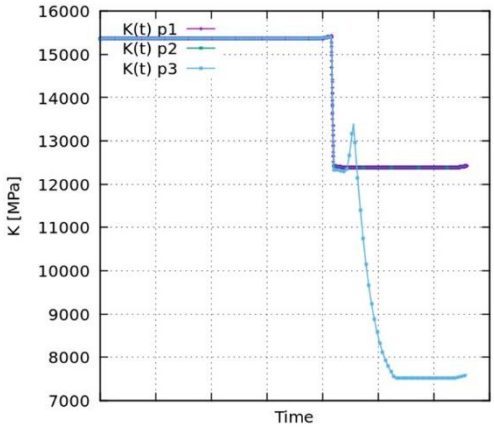

Figure 7. Compressibility modulus over time (Loading-unloading-carbonation-loading-failure)

The q - ε graph is shown in Figure 8. The first mechanical load reaches the yield surface, damaging the sample and reducing the mechanical modulus (Eq. 17). After unloading, the carbonation modifies the stress state of the sample and the bulk modulus as well. This causes the slope of the curve to be lower and the ultimate strength to be lower as well.

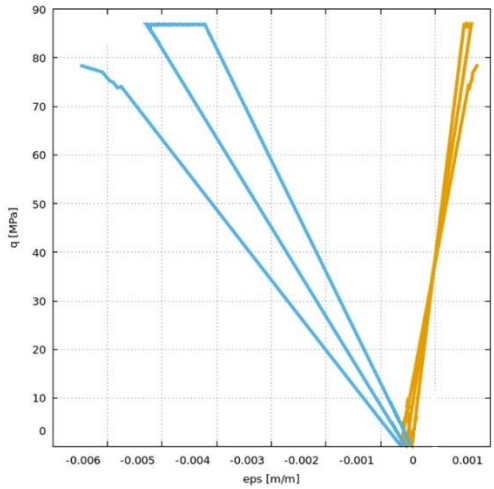

Figure 8. deviatoric stress (q) vs. strains (eps). The light blue line corresponds to the axial strain, while the brown line corresponds to the radial strain (Loading-unloading-carbonation-loading-failure).

5 CONCLUSIONS

Preliminary results were obtained on samples with bacterial nanocellulose after a supercritical carbonation at 20 MPa and at 90°C for 30 days.

Isotropic drained and undrained tests were performed to obtain the compressibility moduli of carbonated cement samples.

A chemo-hydro-mechanical coupled model was used to simulate the carbonation test and the triaxial tests. Additionally, an implementation of isotropic damage was used to calculate the variation of the bulk modulus after carbonation and mechanical loadings.

Samples with bacterial nanocellulose show an increase in elastic properties since the drained and undrained compressibility moduli are higher than cement with no additions. After carbonation, the elastic properties are reduced, but the

modified samples present higher modulus than carbonated cement samples.

The results obtained show that the bacterial nanocellulose could be used as an additive to improve cement properties and resist cement carbonation.

6 REFERENCES

API Specification 10A, 2019. Specification for Cements and Materials for Well Cementing, Twenty-Fif. ed, American Petroleum Institute. Northwest Washington, DC.

Barría, J.C., Manzanal, D., Pereira, J.M., 2019. CO2 Geological Storage: Performance of Cement-Rock Interface, in: Proceedings of the XVI Pan-American Conference on Soil Mechanics and Geotechnical Engineering (XVI PCSMGE). Cancún, pp. 2873–2881. https://doi.org/10.3233/STAL190359

Barría, J.C., Manzanal, D., Pereira, J.M., Ghabezloo, S., 2020a. CO2 geological storage: Microstructure and mechanical behavior of cement modified with a biopolymer after carbonation. E3S Web Conf. 205. https://doi.org/10.1051/e3sconf/202020502007

Barría, J.C., Manzanal, D.G., Martín, C.M., Piqué, T., Pereira, J.M., 2020b. Cement-rock interface subjected to SCCO2, in: Rock Mechanics for Natural Resources and Infrastructure Development-Proceedings of the 14th International Congress on Rock Mechanics and Rock Engineering, ISRM 2019. pp. 3196–3203.

Barría, J.C., Vázquez, A., Pereira, J.M., Manzanal, D., 2021. Effect of bacterial nanocellulose on the fresh and hardened states of oil well cement. J. Pet. Sci. Eng. 199. https://doi.org/10.1016/j.petrol.2020.108259

Barria, JC; Martin, C.; T. Pique; JM Pereira; D. Manzanal (2018) Analysis of modified cement paste in the context of CO2 geological storage. International Symposium of Energy Geotechnics. Lugar: Laussane Pages 402-409; https://doi.org/10.1007/978-3-319-99670-7 . Publisher: Springer, Cham. Online ISBN 978-3-319-99670-7

Coussy, O., 2010. Mechanics and Physics of Porous Solids, Mechanics and Physics of Porous Solids. https://doi.org/10.1002/9780470710388

Dangla, P., Bonnard, A., 2017. Ifsttar/bil: first version in github (Version v2.4). Zenodo. https://doi.org/10.5281/zenodo.1039729

Fernández Bertos, M., Simons, S.J.R., Hills, C.D., Carey, P.J., 2004. A review of accelerated carbonation technology in the treatment of cement-based materials and sequestration of CO2. J. Hazard. Mater. 112, 193–205. https://doi.org/10.1016/j.jhazmat.2004.04.019

Gatenholm, P., Klemm, D., 2010. Bacterial Nanocellulose as a Reneable Material for Biomedical Applications. MRS Bull. 35, 208–213. https://doi.org/10.1080/15440478.2018.1439426

Ghabezloo, S., Sulem, J., Guédon, S., Martineau, F., Saint-Marc, J., 2008. Poromechanical behaviour of hardened cement paste under isotropic loading. Cem. Concr. Res. 38, 1424–1437. https://doi.org/10.1016/j.cemconres.2008.06.007

Ghabezloo, S., Sulem, J., Saint-Marc, J., 2009. Evaluation of a permeability-porosity relationship in a low-permeability creeping material using a single transient test. Int. J. Rock Mech. Min. Sci. 46, 761–768. https://doi.org/10.1016/j.ijrmms.2008.10.003

Gómez Hoyos, C., Cristia, E., Vázquez, A., 2013. Effect of cellulose microcrystalline particles on properties of cement based composites. Mater. Des. 51, 810–818. https://doi.org/10.1016/j.matdes.2013.04.060

Hisseine, O.A., Omran, A.F., Tagnit-Hamou, A., 2018. Influence of cellulose filaments on cement paste and concrete. J. Mater. Civ. Eng. 30, 1–14. https://doi.org/10.1061/(ASCE)MT.1943-5533.0002287

Kachanov, L., 1971. Introduction to Continuum Damage Mechanics.

Kutchko, B.G., Strazisar, B.R., Lowry, G.V., Dzombak, D. a., Thaulow, N., 2008. Rate of CO2 Attack on Hydrated Class H Well Cement under Geologic Sequestration Conditions. Environ. Sci. \& Technol. 42, 6237–6242. https://doi.org/10.1021/es800049r

Mainguy, M., 1999. modeles de diffusion non-lineaires en milieux poreux. Applications a la dissolution et au sechage des materiaux cimentaires.

Mejdoub, R., Hammi, H., Suñol, J.J., Khitouni, M., Boufi, S., 2017. Nanofibrillated cellulose as nanoreinforcement in Portland cement : Thermal , mechanical and microstructural properties. J. Compos. Mater. 51, 2491–2503. https://doi.org/10.1177/0021998316672090

Morandeau, A., Thiéry, M., Dangla, P., 2014. Investigation of the carbonation mechanism of CH and C-S-H in terms of kinetics, microstructure changes and moisture properties. Cem. Concr. Res. 56, 153–170. https://doi.org/10.1016/j.cemconres.2013.11.015

Philip Ringrose, 2020. How to Store CO2 Underground: Insights from early-mover CCS Projects. Springer.

Samudio, M., 2018. Modelling of an oil well cement paste from early age to hardened state : hydration kinetics and poromechanical behaviour To cite this version : Université Paris-Est.

Ulm, F.J., Constantinides, G., Heukamp, F.H., 2004. Is concrete a poromechanics material? - A multiscale investigation of poroelastic properties. Mater. Struct. Constr. 37, 43–58. https://doi.org/10.1617/14100

Vallin, V., 2014. Modélisation chimio poromécanique du comportement des géomatériaux dans le contexte du stockage géologique du dioxyde de carbone : Application au puits d'injection. Université Paris-Est.

Vallin, V., Pereira, J.M., Fabbri, A., Wong, H., 2013. Numerical modelling of the hydro-chemo-mechanical behaviour of geomaterials in the context of CO 2 injection 3052–3069. https://doi.org/10.1002/nag

Xu, B., Yuan, B., Wang, Y., Zeng, S., Yang, Y., 2019. Nanosilica-latex reduction carbonation-induced degradation in cement of CO2 geological storage wells. J. Nat. Gas Sci. Eng. 65, 237–247. https://doi.org/10.1016/j.jngse.2019.03.013